Available online at www.sciencedirect.com
SCIENCE DIRECT®
International Journal of Pharmaceutics xxx (2005) xxx–xxx
international journal of pharmaceutics
www.elsevier.com/locate/ijpharm

Thermal behaviour and stability in Olanzapine

Griselda I. Polla [a], Daniel R. Vega [a,*], Hilda Lanza [a], Dora G. Tombari [b], Ricardo Baggio [a], Alejandro Pedro Ayala [d], Josué Mendes Filho [d], Daniel Fernández [a], Gabriela Leyva [a], Gustavo Dartayet [c]

[a] *Unidad de Actividad Física, Comisión Nacional de Energía Atómica, Av. Gral. Paz 1499, San Martín, 1650 Buenos Aires, Argentina*
[b] *Gador S.A. Div. Farmacoquímica—Calle 10—Parque Industrial Pilar, 1629 Buenos Aires, Argentina*
[c] *Laboratorios Beta S.A., Bouchard 3122, Lanús Este, Buenos Aires, Argentina*
[d] *Departamento de Física, Universidade Federal do Ceará, Caixa Postal 6030, 60.455-970 Fortaleza, CE, Brazil*

Received 1 February 2005; received in revised form 5 May 2005; accepted 5 May 2005

Abstract

The stability and thermal behaviour of two anhydrate phases and a new mixed water:DMSO solvate of Olanzapine (2-methyl-4-(4-methyl-1-piperazinyl)-10H-thieno-[2,3-b][1,5]benzodiazepine) are studied by different methods: differential scanning calorimetry (DSC), X-ray powder diffraction (XRPD) and Raman scattering (RS). Single crystal structural data for the latter phase are presented, confirming the presence of the $(Olanzapine)_2$ dimer as the structural building unit of all known phases of the drug, either anhydrate or solvated.

An apparent interconversion between both solid state forms is shown to be an artifact and explained in terms of a melting–recrystallization process.
© 2005 Elsevier B.V. All rights reserved.

Keywords: Olanzapine; Polymorphism; Stability

1. Introduction

Olanzapine (2-methyl-4-(4-methyl-1-piperazinyl)-10H-thieno-[2,3-b][1,5]benzodiazepine) is a relatively new benzodiazepine which has been found useful in the treatment of, among other psychosis, schizophrenia (Dossenbach et al., 2004; Heresco-Levy et al., 2004; Sclar et al., 2003). In the last few years its pharmaceutical relevance prompted an intense research work regarding the different solid state phases of the compound. In particular, in a very complete report on the subject (Reutzel-Edens et al., 2003) three different anhydrides, three dihydrated forms, a higher hydrate and an undisclosed number of mixed solvates have been identified and characterized.

* Corresponding author. Tel.: +54 11 6772 7107; fax: +54 11 6772 7121.
E-mail address: vega@cnea.gov.ar (D.R. Vega).

0378-5173/$ – see front matter © 2005 Elsevier B.V. All rights reserved.
doi:10.1016/j.ijpharm.2005.05.035

The fact that fractions of all three anhydrates could be obtained from desolvation of different hydrates, or that two of them could convert into a third one through temperature driven processes suggested that a common packing pattern might be present, and that the many different structures in which the compound crystallizes probably differ only slightly in their packing arrangement, irrespective of the solvate content. The crystal structure resolution of a stable anhydrate and several solvated forms supplied a partial answer to this issue, as in all of them the racemic compound paired both opposite chiral moieties into almost identical dimeric units, built up around a symmetry centre and stabilized by internal, weak non-bonding interactions. These aggregates would in turn act as the elemental building blocks for the structural assembly. The hypothesis posed new interesting questions about the stability of the different crystalline phases as well as the characteristics of the transitions involved in the transformation processes, in particular, those which do not involve mass loss but just a packing reshuffling, as were expected to be the ones interconverting unsolvated forms of the compound.

In the present work we have focused our interest on the stability of the two Olanzapine anhydrate phases of commercial relevance, viz., those named I and II in Reutzel-Edens et al. (2003), but contradicting the original patent (US Patent, 1997) which labels them exactly the opposite. In order to avoid confusion we shall call them **(1)** and **(2)**, respectively. The extra anhydrous phase therein reported as III appeared only as an elusive desolvation product, and was accordingly disregarded from our study. During the many crystallization attempts a new, unreported water–DMSO solvate was generated (to be referred to as **(3)**), the crystal structure of which is also presented.

The behaviours of **(1)** and **(2)** (and incidentally, **(3)**) were scrutinized as a function of time and temperature, and fully characterized through differential scanning calorimetry (DSC), X-ray powder diffraction (XRPD) and Raman spectroscopy (RS). The latter technique was chosen as a probe of the low energy vibrational modes, directly related to the crystal packing, and thus extremely sensitive for crystal phase discrimination.

The combined results of all these techniques as applied to the unsolvated forms **(1)** and **(2)**, and the new mixed solvate **(3)** are reported herein.

2. Experimental

2.1. Materials

Polycrystalline samples of the anhydrous polymorphic forms **(1)** and **(2)** of Olanzapine were obtained from Gador and Beta laboratories. Recrystallization from different anhydrous organic solvents, with optimization of growth parameters, were attempted but the efforts to obtain single crystals were only successful in the case of form **(1)**, where slow evaporation of an anhydrous methanolic solution yielded specimens suitable for single crystal X-ray analysis. Though the attempts to obtain single crystals of form **(2)** were systematically unsuccessful, as a by product of these trials single crystals of a new water:DMSO solvate, **(3)**, were obtained by direct crystallization from wet raw material.

2.2. Methods

Single crystal X-ray diffraction data were collected at room temperature with a Siemens R3m diffractometer, with graphite monochromatized Mo Kα radiation, while temperature dependent X-ray powder diffraction data were gathered with Ni-filtered Cu Kα radiation on a digitalized Philips PW1080 diffractometer, equipped with an NMR Technologies, K20 heating stage.

Programs used throughout the crystal resolution and refinement processes: SHELXS, SHELXL (Sheldrick, 1997), SHEXLTL/PC (Sheldrick, 1994). Full use of the crystallography data base at the CCDC (Allen, 2002) was also made for comparison purposes. Crystallographic data (excluding structure factors) for compound **(3)** have been deposited with the Cambridge Crystallographic Data Centre as supplementary publications No. CCDC 249078.

Differential scanning calorimetry was performed in a Shimadzu DSC-60 equipment using dry N_2 as purge gas, with a flow of 30 ml/min and a scan rate ranging from 2 to 10 °C/min.

Thermogravimetric analysis was performed in a Shimadzu DTG-50 equipment, using dry air with a flow of 40 ml/min and a scan rate of 10 °C/min.

The long term stability of the different polymorphs was confirmed following the X-ray diffraction diagrams as a function of time (keeping samples at 60 °C), both when unperturbed and after illuminating them with UV radiation.

Optical microscopy studies were performed on a Leitz Ortholux II Pol-BK polarizing microscope equipped with a Koflerheating stage and an on-purpose adapted webcam. Raman spectra were recorded with a Jobin Yvon T64000 spectrometer, equipped with a N_2-cooled charge-coupled device detector, using the 514.5 nm line of an Argon laser, with a power lower than 5 mW on the sample surface.

3. Results

3.1. Structure analysis

As stated, single crystals could only be obtained for one of the polymorphic anhydratres **(1)** and a mixed water–DMSO solvate **(3)**. Both crystal structures were determined by single crystal X-ray diffraction methods. The one for **(1)** replicated, within experimental error the results already reported in Reutzel-Edens et al. (2003) and Wawrzycka-Gorczyca et al. (2004a), and no specific details will be given here. The structure determination of **(3)** showed it to be a new, mixed (1:0.40) H_2O:DMSO solvate, and to be isostructural to three other ones in the literature, viz., one of the many dehydrates reported in Reutzel-Edens et al. (2003), a pure methanol solvate (Wawrzycka-Gorczyca et al., 2004b) and a mixed (1:1) H_2O:methanol one (Capuano et al., 2003).

The solvato water molecule lays in a fully occupied general position and it is well behaved, while the depleted DMSO unit shows some disorder around a two-fold axis. Since a split model for the DMSO solvate produced unstable results the molecule was refined as laying in the special position, bisected by the rotation axis. This produced a much smoother refinement, though at the cost of large anisotropic displacement factors (in particular for the sulfur atom). Accordingly, the highly prolate ADP reported should not be considered as representing genuine out-of-axis vibrations but just as a means of efficiently taking into account the disorder.

The structure of **(3)** shares the characteristics of all Olanzapine solvates, that is to say they are built up through the piling of $(Olanzapine)_2$ centrosymmetric dimers (Fig. 1), staked into columns parallel to the crystallographic *a* direction, and connected with each other through solvate-mediated interactions. Table 1 presents some relevant crystallographic and refinement data, and Table 2, selected structural parameters.

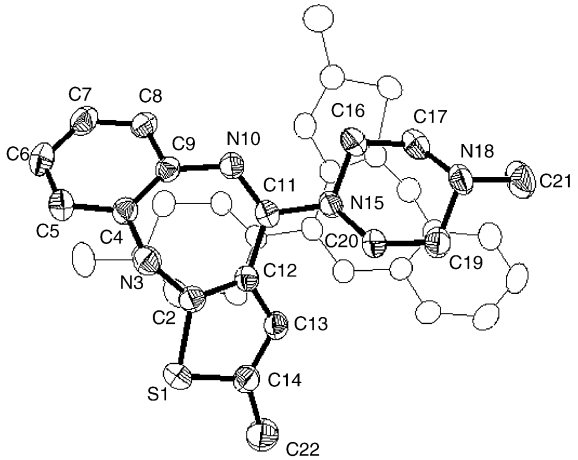

Fig. 1. Molecular diagram of structure **(3)** showing the dimeric unit (solvates omitted). In bold, the independent part (40% probability ellipsoids) showing the numbering scheme used. In light lining, the symmetry related half.

The persistence of the dimeric motive along the series of different Olanzapine structures (either anhydrate or solvated) merits some attention.

In spite of the rather weak interactions involved in connecting the molecular pairs, mainly C–H···π, π···π, etc., the arrangement keeps almost unchanged throughout a variety of packing environments, confirming its intriguing efficiency in what could be consider a leading case of molecular recognition. We have analyzed the extent of this persistency by way of a least squares fit (XP in SHELXTL/PC) of the dimer herein described and all other Olanzapine dimeric units reported in the literature. The results could not be more surprising: the largest discrepancy, found with the anhydrate, presented an average atomic deviation as small as 0.38 Å. On the other hand, the best fit, occurred, as expected, with one of the isostructural solvates, and presented a mean deviation of 0.19 Å.

Both cases are presented in Fig. 2a and b, respectively.

As a way to assess the validity of one such comparison, the three different resolutions of Olanzapine anhydrate available to us (the ones in Reutzel-Edens et al. (2003), Wawrzycka-Gorczyca et al. (2004a) and our own results) were compared through the same method.

Table 1
Crystal data and structure refinement for **(3)**

Empirical formula	$C_{17}H_{20}N_4S$, H_2O, $0.35(C_2H_6OS)$
Formula weight	356.84
Temperature	293(2) K
Wavelength	0.71073 Å
Crystal system	Monoclinic
Space group	*C*2/*c*
a	24.584(4) Å
b	12.5340(19) Å
c	15.153(3) Å
β	125.454(10)°
Volume	3803.5(10) Å^3
Z	8
Density (calculated)	1.246 g/cm^3
Absorption coefficient	0.222 mm^{-1}
F(0 0 0)	1519
Crystal size	0.30 mm × 0.10 mm × 0.10 mm
θ range for data collection	1.92–25.00°
Index ranges	$0 \le h \le 29$, $0 \le k \le 14$, $-18 \le l \le 14$
Reflections collected	3436
Independent reflections	3339 [*R*(int) = 0.0278]
Completeness to *θ* = 25.00°	99.8%
Absorption correction	None
Refinement method	Full-matrix least-squares on F^2
Data/restraints/parameters	3339/2/233
Goodness-of-fit on F_2	1.030
Final *R* indices [*I*>2sigma(*I*)]	$R_1 = 0.0573$, $wR_2 = 0.1311$
R indices (all data)	$R_1 = 0.0958$, $wR_2 = 0.1499$
Largest differential peak and hole	0.649 and −0.370 e Å^{-3}

Table 2
Selected bond lengths [Å] for **(3)**

S(1)—C(2)	1.725(3)
S(1)—C(14)	1.735(4)
C(2)—C(12)	1.359(4)
C(2)—N(3)	1.401(4)
N(3)—C(4)	1.424(4)
C(4)—C(5)	1.388(4)
C(4)—C(9)	1.400(4)
C(5)—C(6)	1.382(5)
C(6)—C(7)	1.374(5)
C(7)—C(8)	1.375(4)
C(8)—C(9)	1.399(4)
C(9)—N(10)	1.404(4)
N(10)—C(11)	1.293(4)
C(11)—N(15)	1.382(4)
C(11)—C(12)	1.473(4)
C(12)—C(13)	1.434(4)
C(13)—C(14)	1.348(4)
C(14)—C(22)	1.507(5)
N(15)—C(16)	1.458(4)
N(15)—C(20)	1.464(4)
C(16)—C(17)	1.512(4)
C(17)—N(18)	1.461(4)
N(18)—C(19)	1.458(4)
N(18)—C(21)	1.475(4)
C(19)—C(20)	1.508(4)

The extreme values for the worst/best agreements were 0.0059/0.0048 Å, indicating a high degree of confidence for the method.

3.2. Raman scattering

Raman spectra of forms **(1)** and **(2)** of Olanzapine are shown in Fig. 3, where four clearly discriminated regions, (a)–(d), can be observed:

Region (d): this is the high frequency zone of C–H modes covering 2700–3100 cm^{-1} and to which many C–H groups contribute (benzene C–H's, piperazine C–H_2's, methyl C–H_3's, etc.). In this region, bands differ both in intensities as well as in position.

Region (c): this is the medium frequency zone corresponding to C–C modes, located between 1500 and 1700 cm^{-1}. To the energy shift characteristic of C–H modes, C–C ones add the splitting of some bands. Due to the fact that this is not an effect common to all but only to a few bands the effect cannot be ascribed to an increase in the number of independent molecules, but more probably to the lowering of the site symmetry of some functional groups. This conclusion is supported by ^{13}C and ^{15}N solid state nuclear magnetic resonance measurement reported in Reutzel-Edens et al. (2003).

Region (b): by decreasing the energy of the vibrational modes, the rest of the *fingerprint* region (600–1700 cm^{-1}) provides several features that may be used to distinguish between both crystalline forms.

Region (a): but it is in this low wavenumber region (below 400 cm^{-1}, where backbone deformations, librations and lattice vibrations appear), that the potentiality of the method as applied to phase differentiation is more evident. In fact, we have used the crystal packing sensitivity of these vibrational modes in order to investigate the thermal stability of **(2)**, as a complementary study to those performed by alternative techniques. The temperature dependence of the Raman spectra of form **(2)** is shown in Fig. 4. Between room temperature and 150 °C no evident changes in

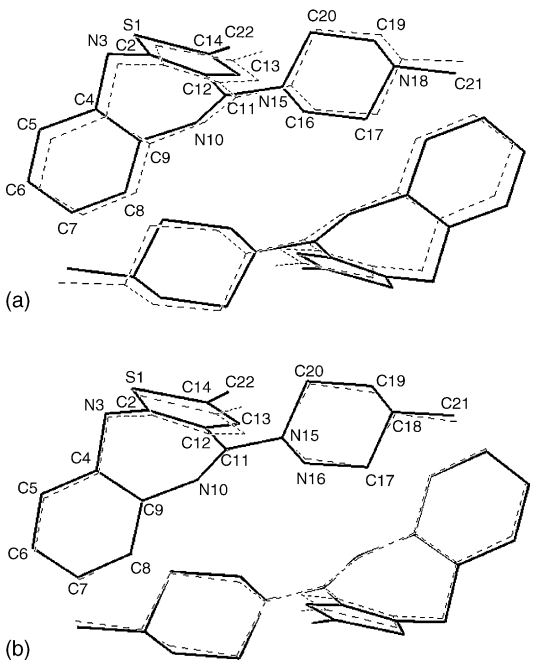

Fig. 2. Least squares overlap showing the worst agreement between two different dimeric units (a) the one in **(3)** vs. the one reported in Wawrzycka-Gorczyca et al. (2004a); (b) the one in **(3)** vs. the one reported in Capuano et al. (2003).

the lattice modes may be identified, confirming that form **(2)** remains stable until this temperature. However, at 160 °C some new features alert about the onset of a phase transition: two small shoulders located at ∼25 and ∼100 cm^{-1} grow dramatically as the temperature rises up to 180 °C.

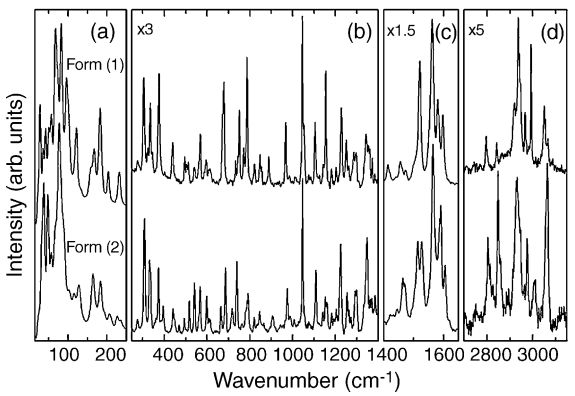

Fig. 3. Raman spectra of forms **(1)** and **(2)**.

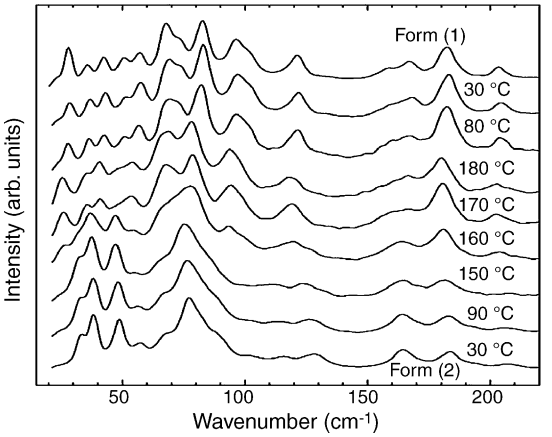

Fig. 4. Temperature dependence of the Raman spectra of form **(2)**. Temperatures are given in chronological order. The room temperature Raman spectrum of form **(1)** is included for comparison.

This should be correlated with the results presented in the following section; the fact that the onset involved appears as shifted might probably be attributed to the laser probe introducing some local extra energy, not accounted for by the temperature testing device.

The following two spectra in Fig. 4, taken (while cooling) at 70 and 30 °C show that the process does not revert; comparison with the one on top (corresponding to form **(1)** at room temperature) confirms the phase transformations from form **(2)** to form **(1)**.

3.3. Thermal studies (XRPD and DSC)

The XRPD diagrams of forms **(1)** and **(2)** are shown in Fig. 5 Important differences are clearly visible, mainly in the peaks at $2\theta = 8.6°$, 12.4°, 14.4° and 16.9°, and which can therefore serve as useful discriminators for form **(1)**.

DSC studies of both anhydrous forms presented different thermal behaviours as shown in Fig. 6a and b.

Both diagrams show endothermic peaks, none of which is related to weight loss as checked by TG analysis. In both cases the transition with T_{onset} about 194 °C is related to the final melting of both samples, with a similar latent heat ($\Delta H_{(1)-Liq}$) of about 143 J/g. For structure **(1)** this is the only anomaly in the thermal behaviour.

Structure **(2)** shows instead a second endothermic peak with T_{onset} about 177 °C and an exothermal signal

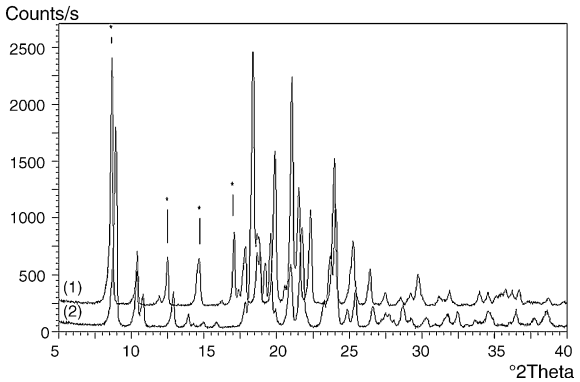

Fig. 5. XRPD diagrams of forms **(1)** and **(2)**. Characteristic peaks of form **(1)** were marked with *.

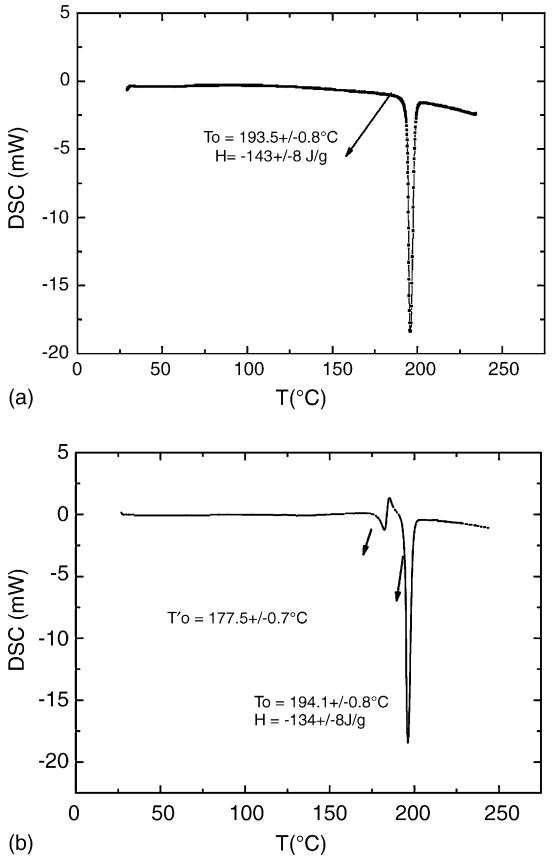

Fig. 6. Differential scanning calorimetry diagrams (a) of structure **(1)**; (b) of structure **(2)**.

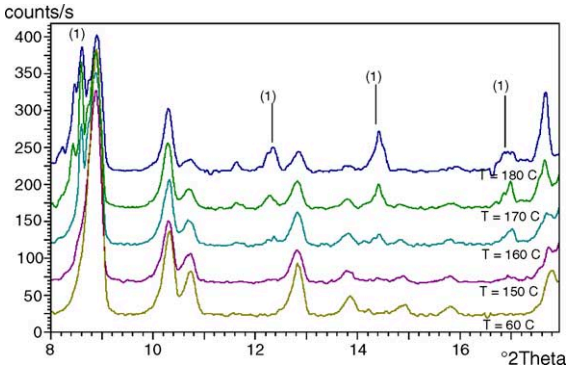

Fig. 7. X-ray powder diffraction diagrams of form **(2)** taken as a function of temperature from 60 to 180 °C. Characteristic reflections of form **(1)** are indicated.

partially superposed to the latter; even at scanning rates as low as 2 °C/min these two processes could not be isolated. By cycling the samples between room temperature and $T = 180$ °C no signs of reversibility of these transitions could be observed. X-ray powder diffraction diagrams taken as a function of temperature showed this process to be associated with the appearance of form **(1)** coexisting with form **(2)** in the temperature range 160–180 °C (Fig. 7). Monitoring this transition in the optical microscope with a digital camera showed the appearance of small isolated crystallites in the originally finely powdered sample, though no signs of local melting were visually evident.

A satisfactory explanation for these facts can be given considering **(1)**–**(2)** as a dimorphic monotropic system (see Bernstein (2002) for details). Fig. 8

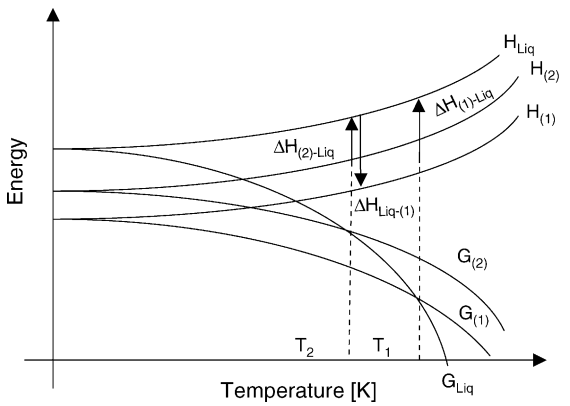

Fig. 8. Energy vs. temperature diagram for a dimorphic monotropic system.

presents a schematic energy versus temperature diagram for such a case, where the three pairs of divergent curves represent the individual behaviours of the enthalpy (H) and the Gibbs free energy (G) for forms **(1)**, **(2)** and the liquid phase.

In this diagram the $G_{(2)}$ values for modification **(2)** stay above the corresponding ones for **(1)** all over the RT–T_2 (ca. 170 °C) range. The fact that our samples of form **(2)** kept stable at RT for long periods of time (ca. 1 year) can be interpreted as meaning that the energy barrier between both forms is high enough as to render the spontaneous inter conversion process in the solid state unlikely or, at least, the transformation kinetics quite slow. At ca. 170 °C (T_2 in Fig. 8) the Gibbs free energy of the liquid phase G_{liq} becomes smaller than the one for **(2)** and melting of this form occurs (endothermic peak in the DSC). However, at this temperature form **(1)** is thermodynamically more stable than the melt ($G_{(1)} < G_{liq}$), and immediate solidification of **(1)** occurs (exothermic peak in the DSC, almost superposed to the former one).

The integrated endo + exo peaks in the T_2 zone of the DSC diagram (in Fig. 8: $\Delta H_{(2)-Liq} + \Delta H_{Liq-(1)} = \Delta H_{(2)-(1)} \approx 0.4(2)$ J/g) ought to be a measure of the enthalpy (and accordingly of the stability) difference between both modifications.

The melting + recrystallization process is so fast as to preclude its visualization by optical means, but the clear morphological change from a finely grained texture below T_2 to one with distinct crystallites above T_2 strongly supports the argument.

The surprising immediacy of this transformation might well be due to the eventual presence of undetectable amounts of form **(1)** in the bulk of form **(2)**, and which would act as seeds triggering the recrystallization process.

Above this temperature the only modification present is form **(1)** (as confirmed by XRD and Raman), stable up to T_1 where the G_{liquid} curve falls below $G_{(1)}$ and final melting takes place.

In the case of the water–DMSO solvate **(3)**, its thermal behaviour (Fig. 9) showed some processes related to the complete desolvation of the sample (weight loss = 13%, expected from X-ray refinement = 12.7%). The melting temperature is about 193 °C and the heat of fusion (corrected by the previous weight loss) is about 126 J/g, suggesting that also in this case form **(1)** is obtained after desolvation. Also in this case the assumption was checked by an X-ray diffraction, this time on quenched samples.

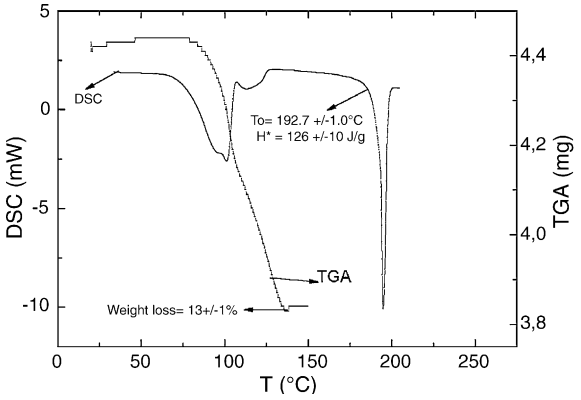

Fig. 9. Differential scanning calorimetry diagram of water–DMSO solvate **(3)**.

4. Conclusions

The present results could be considered as a quantitative improvement to many qualitative results already present in the pioneering works on the subject, viz.:

(a) There are in Olanzapine crystal phases a structural building block conformed by a dimeric unit which is quite "rigid" irrespective of packing environment and in spite of the weak interactions involved in its stability (we have enlarged the series of examples with the structure of a new solvate).
(b) There is a different thermal behaviour in the two most common anhydrate forms: form **(1)** (which crystal structure we have re-confirmed by single crystal X-ray diffraction) does not present any thermal anomaly up to the melting point. Form **(2)**, instead, presents a (seemingly) more complex behaviour, but which can be easily explained considering **(1)**–**(2)** a dimorphic monotropic system: our results confirm that form **(1)** is the stable one in the solid state, as reported by Reutzel-Edens et al. (2003), and that the apparently puzzling "interconversion" between both forms is in fact just a melting process followed by an almost immediate recrystallization.

As a final remark, it is perhaps worth emphasizing that most of the conclusions attained were the result of

a combined analysis of complementary data obtained through a number of multidisciplinary techniques (single crystal XRD, powder XRD, DSC, Raman scattering, etc.), none of which, on its own means, could have provided a definite answer to any of the questions posed.

Acknowledgements

We acknowledge CONICET funding through project PIP 2367/00 and the Spanish Research Council (CSIC) for provision of a free-of-charge license to the CSD system (Allen, 2002).

References

Allen, F.H., 2002. Acta Crystallogr. B58, 380.
Bernstein, J., 2002. Polymorphism in Molecular Crystals. Clarendon Press, Oxford (Chapter 2).
Capuano, B., Crosby, I.T., Fallon, G.D., Lloyd, E.J., Yuriev, E., Egan, S.J., 2003. Acta Crystallogr. E 59, o1367.
Dossenbach, M.R.K., Folnegovic-Smalc, V., Hotujac, L., Uglesic, B., Tollefson, G.D., Grundy, S.L., Friedel, P., Miro Jakovljevic, M., 2004. Prog. Neuropsychopharmacol. Biol. Psychiatry 28, 311–318.
Heresco-Levy, U., Ermilov, M., Lichtenberg, P., Bar, G., Javitt, D.C., 2004. Biol. Psychiatry 55, 165–171.
Reutzel-Edens, S., Bush, J.K., Magee, P.A., Sephenson, G., Byrn, S.R., 2003. Cryst. Growth Des. 3, 897–907.
Sclar, D.A., Skaer, T.L., Robison, L.M., Dickson, W.M., Markowitz, J.S., De Vane, C.L., 2003. Eur. Neuropsychopharmacol. 13, S281–S282.
Sheldrick, G.M., SHELXTL-PC. Version 5.0, Siemens Analytical X-ray Instruments Inc., Madison, Wisconsin, USA, 1994.
Sheldrick, G.M., 1997. SHELXS-97 and SHELXL-97—Programs for Structure Resolution and Refinement. University of Göttingen, Germany.
U.S. Patent No. 5631250, 20 May 1997.
Wawrzycka-Gorczyca, Koziol, A.E., Glice, M., Cybulski, J., 2004a. Acta Crystallogr. E 60, o66.
Wawrzycka-Gorczyca, I., Mazur, L., Koziol, A.E., 2004b. Acta Crystallogr. E 60, o69.